

## **Automated Cloud Detection and Typing of Data Collected by the Visible Infrared Imager Radiometer Suite (VIIRS)**

Keith Hutchison<sup>\*</sup>, John Roskovensky<sup>#</sup>, John Jackson<sup>#</sup>, Andrew Heidinger<sup>+</sup>, Michael Pavolonis<sup>&</sup>, Richard Frey<sup>&</sup>, and Thomas Kopp<sup>\$</sup>

### **ABSTRACT**

The Visible Infrared Imager Radiometer Suite (VIIRS) is the high-resolution Earth imager of the United States National Polar-orbiting Operational Environmental Satellite System (NPOESS). VIIRS has its heritage in three sensors currently collecting imagery of the Earth, including NOAA's Advanced Very High Resolution Radiometer, NASA's Moderate Resolution Imaging Spectroradiometer, and the DoD's Operational Linescan Sensor flown by the Defense Meteorological Satellite Program. First launch of the VIIRS sensor comes on NASA's NPOESS Preparatory Project (NPP) in late 2006. Data collected by the VIIRS sensor will provide products to a variety of users in the DoC, DoD, and at NASA that support applications from the real-time to long-term, climate change timescales. VIIRS has been uniquely designed to satisfy this full range of requirements. Cloud masks derived from the automated analyses of VIIRS data are critical data products for the NPOESS program and the retrieval algorithms have been designed to exploit the unique sensor data collected by the VIIRS instrument. In this paper, the VIIRS Cloud Mask (VCM) performance requirements are highlighted, along with the algorithmic logic developed to satisfy these requirements. The expected performance for the VCM algorithm is established using global synthetic cloud simulations and manual cloud analyses of VIIRS proxy imagery. These results show the

VCM analyses will satisfy the performance expectations of products created from it, including land and ocean surface products, cloud microphysical products, and automated cloud forecast products. Finally, minor deficiencies that remain in the VCM algorithm logic are identified along with a mitigation plan to resolve each prior to NPP launch or shortly thereafter.

---

Corresponding Author: Keith Hutchison, Center for Space Research (CSR), The University of Texas at Austin, 3925 W. Braker Lane, Ste. 200, Austin, TX 78759, [keithh@csr.utexas.edu](mailto:keithh@csr.utexas.edu), (512)-471-7295

John Roskovensky and John Jackson, Northrop Grumman Space Technology (NGST), NPOESS System Engineering, Modeling & Simulations, One Space Park, Redondo Beach, CA 90245

Andrew Heidinger, NOAA National Environmental Satellite, Data, and Information Service (NESDIS) Office of Research and Applications, 1225 W. Dayton Street, Madison, WI

Michael Pavolonis and Richard Frey, Cooperative Institute for Meteorological Satellite Studies (CIMSS), University of Wisconsin, Madison, WI

Thomas Kopp, The Aerospace Corporation, Offutt Air Force Base, NE.

## 1.0 INTRODUCTION

The National Polar-orbiting Operational Environmental Satellite System (NPOESS) was established by Presidential Decision Directive NSTC-2 on May 5, 1994. This directive required the Departments of Commerce (DoC) and Defense (DoD), and NASA to create an [Integrated Program Office \(IPO\)](#) to develop, acquire, manage, and operate the next generation of polar-orbiting operational environmental satellites for the United States. The NPOESS IPO was established on October 3, 1994 with a mandate that extends to the year 2018. The IPO has partnered with the European Organisation for the Exploitation of Meteorological Satellites ([EUMETSAT](#)) and the National Space Development Agency of Japan ([NASDA](#)) to ensure a long-term continuity of observations from polar orbit will continue to support improvements in the operational meteorological, environmental, and climate monitoring services of its user communities.

NPOESS satellites will carry numerous sensors to collect data from the visible through the microwave regions of the electromagnetic spectrum that will be used to create a large number of data products, also called [environmental data products](#). The [Visible/Infrared Imager Radiometer Suite](#) (VIIRS) is the NPOESS high-resolution Earth viewing sensor. VIIRS has its heritage in three sensors currently collecting imagery of the Earth, including NOAA's Advanced Very High Resolution Radiometer (AVHRR), NASA's MODerate Resolution Imaging Spectroradiometer (MODIS), and the DoD's Operational Linescan Sensor (OLS) flown by the Defense Meteorological Satellite Program (DMSP). Like MODIS, VIIRS will provide highly calibration data in all channels collected using

four-focal plane assemblies. In addition, it relies heavily upon its MODIS and AVHRR heritage for spectral bandpass definitions used in automated cloud detection algorithms. VIIRS also relies upon its DMSP OLS heritage to provide data at edge of scan that grows to no more than twice its spatial resolution at nadir. VIIRS will collect data at two nominal resolutions at nadir: 375 m in “Imagery” channels and 750 m in “Radiometric” channels. Finally, VIIRS contains the legacy to the DMSP nighttime (low light) visible channel, known as the Day-Night Band (DNB). First launch of the VIIRS sensor comes on NASA’s [NPOESS Preparatory Project](#) (NPP) in late 2006.

Data collected by the VIIRS sensor will be used to create nearly 30 environmental data [products](#) including cloud analyses, land and ocean surface products, and aerosol products. These products will be delivered to a diverse [user community](#) in the DoC, DoD, and at NASA that support applications from the real-time to long-term, climate change timescales and VIIRS has been designed to satisfy this full range of requirements.

The cloud mask derived from the automated analysis of VIIRS data is a critical data product for the NPOESS program and has been designed to exploit the unique data collected by the VIIRS sensor. In the next section, the VIIRS Cloud Mask (VCM) performance requirements are highlighted, along with the algorithmic logic developed to satisfy these requirements. Next, the expected performance for the VCM algorithms is established using global synthetic cloud simulations and manual cloud analyses of VIIRS proxy imagery created from MODIS granules. These results show the VCM analyses will satisfy the performance expectations of products created from it, including land and

ocean surface products, cloud microphysical products, and automated cloud forecast products. Finally, minor deficiencies that continue in the VCM algorithms are identified along with a mitigation plan to resolve each prior to NPP launch or shortly thereafter.

## **2.0 VIIRS CLOUD MASK ALGORITHMS**

Stringent requirements have been levied upon the VCM analyses as shown in Table 1, which is taken from the NPOESS System Specification, the document that defines acceptable performance for the total NPOESS system and each sub-system. These requirements vary according to cloud optical thickness (COT) and solar illumination conditions. For example, during daytime conditions, over the ocean, and outside sun glint regions, the VCM algorithms are required to detect 99% of the pixels that contain clouds that are optically thick ( $OD > 0.5$ ) and 92% of more optically thin clouds. Inside regions of sun glint, defined by the reflected sun angle  $< 36$  degrees, the cloud mask must meet nighttime performance requirements of 96% and 90% respectively. For purposes of validation, performance will be based upon manual classification of VIIRS imagery and cloud masks used to generate synthetic data sets, using procedures discussed in Section 3. No other sensor is known to have such stringent performance requirements for cloud analyses.

**Table 1 here.**

## **2.1 VIIRS SENSOR DESIGN ENHANCEMENTS**

The VIIRS sensor was designed to meet the rigorous cloud product performance requirements originally established by the IPO and later incorporated into the NPOESS

System Specification. A summary of VIIRS channel characteristics useful for cloud detection is shown in Table 2 along with those of heritage sensors, VIIRS design enhancements, and the value of each enhancement to the overall performance of the VCM algorithms.

**Table 2 here.**

The VIIRS design contains numerous enhancements to channels used in heritage sensors.

The value of these enhancements can be summarized as follows:

- The M1 band has been proven valuable for cloud detection over arid surfaces in daytime imagery (Hutchison and Jackson, 2003); however, MODIS data can saturate in cloudy conditions. VIIRS channels used for ocean color monitoring, including the M1 channel, are dual-gain to ensure saturation does not occur. As an added precaution, all dual-gain bands and M13 are downlinked at full resolution, i.e. not subject to on-board aggregated as done with single gain bands. (Oversampling and on-board aggregation are used to restrict growth in spatial resolution as VIIRS scans from nadir to edge of swath.)
- VIIRS Channels reflective bands (e.g. I1, I2 etc) are accurately calibrated, compared to its OLS and AVHRR counterparts. The M5 and M7 Channels have a narrow bandpass, similar to MODIS, which reduces global variations in atmospheric transmittance due to changes in viewing geometry and atmospheric conditions. Thus, cloud signatures in these VIIRS bandpasses will also be less variability than observed in data collected by the OLS and AVHRR sensors.

- The bandwidth of VIIRS Channel M9 has been reduced 50%, from 30 nm in MODIS to 15 nm, which will reduce contamination from the Earth's surface that is present in MODIS data. This reduced bandpass will help provide more accurate cloud detection and typing in the presence of lower amounts of atmospheric water vapor, especially associated with polar environments and mountainous regions.
- Data collected in VIIRS channels I4 and I5 have a much higher spatial resolution, i.e. 375 m at nadir compared to 1 km resolution in MODIS data, which reduces sub-pixel effects on VCM analyses.
- Similarly, restrictions on cross-scan spatial resolution growth in VIIRS imagery and radiometric channels to 2:1, compared to almost 6:1 in AVHRR and MODIS further reduces impacts of sub-pixel effects on cloud detection. (This growth applies to a MODIS data swath of 2330 km compared to a VIIRS 3000 km swath, which makes VIIRS data contiguous at the equator.)
- Finally, all VIIRS data, including the DNB, are more highly calibrated than OLS data. This allows VCM algorithms to produce improved cloud analyses even in terminator regions when compared to analyses based upon OLS data which have similar spatial resolution characteristics.

The VIIRS design also provides some data that appear inferior to similar data collected by MODIS. For example, the aforementioned cloud tests that utilize VIIRS imagery channels could be applied more effectively near nadir with MODIS Channel 1, which has a resolution of 250 m. However, this value is quickly lost as the sensor scans away from nadir due to the unconstrained growth of nearly 6:1 in resolution in MODIS compared to

2:1 constraint associated with the VIIRS design. Secondly, MODIS channels, in general, have a higher signal-to-noise ratio (SNR) capability than that found in corresponding VIIRS imagery bands. However, since most cloud signatures are strongly reflective, the lower SNR of VIIRS imagery bands will have little impact of cloud detection accuracy. Finally, VIIRS initially will not include a 6.7  $\mu\text{m}$  water vapor band, which has proven highly valuable for cloud detection in the polar night (Liu et al., 2004). This band is currently being considered for inclusion beginning with VIIRS Flight Unit #3 and those instruments launched thereafter.

## 2.2 VIIRS CLOUD DETECTION ARCHITECTURE

The methodology for multi-spectral, automated cloud detection algorithms follows closely that first described in the literature by Saunders and Kriebel (1988) which formed the theoretical basis for APOLLO or Processing scheme Over Land, Clouds, and Ocean (Kriebel et al 2003), CLAVR (CLouds from AVHRR by Stowe et al., 1999; Heidinger, 2004), SERCCA (Support of Environmental Requirements for Cloud Analyses and Archive by Gustafson et al., 1994), and the MODIS cloud mask algorithms (Ackerman et al., 1997; Ackerman et al., 1998; Ackerman et al., 2002). The architecture of the VCM algorithms, which is shown in Figure 1 for daytime conditions, follows closely that of MODIS. (The architecture of the nighttime algorithm is not shown since it is more simplistic than that used in the daytime algorithm.)

**Figure 1 here.**

Multispectral cloud detection algorithms normally start with the assumption that each pixel is cloud-free. Then, depending upon the pixel location with respect to a geographic database, a set of spectral and bi-spectral cloud tests are employed to exploit the different signatures of clouds and their surrounding backgrounds. If the sensor observations exceed a predetermined value or “threshold” for any single cloud test, the pixel is assumed to be cloud-contaminated. The goal of each cloud test is to maximize the number of cloudy pixels detected while simultaneously minimizing the number of cloud-free pixels inaccurately classified as cloud contaminated, i.e. minimizing false alarms. Multispectral cloud detection algorithms may also incorporate single-channel cloud tests; however, care must be taken since cloud and background signatures are highly variable in global satellite observations and these variations may be difficult to describe in the logic available with a single spectral band. Shown in Table 3 are cloud tests used in the VCM daytime algorithm. (Note: units in Table 3 are reflectance (R) for solar bands in percent and brightness temperatures (BT) for emissive bands in degrees Kelvin. Brightness temperature differences (BTD) are also in degrees Kelvin.)

**Table 3 here.**

There are currently four cloud tests unique to the VCM algorithms, i.e. not used in the corresponding MODIS algorithms. These tests (11 - 14) were either created specifically for the VIIRS Cloud Mask Algorithm (Hutchison and Jackson, 2003) or have a heritage in the CLAVR Cloud Mask Algorithms (Heidinger, 2004). They were added to resolve two major class problems identified during initial verification testing of the VIIRS

algorithms in early 2003, which will be discussed in Section 4.1. These problems included:

- Unacceptable “leakage” rates over water (ocean) surface, i.e. clouds present in the truth data were not detected by the VCM algorithms, and
- Unacceptable “false alarm” rates over land surfaces, i.e. pixels not classified as cloudy in the truth data were classified as cloudy by the VCM algorithms.

The VCM algorithms output a cloud confidence based upon results of the cloud tests shown in Table 3. Possible cloud confidences are confidently clear, probably clear, probably cloudy, and confidently cloudy. A binary cloud mask results by grouping together both classes of cloudy pixels and separately both classes of clear pixels. Confidences are established based upon the proximity of sensor observations to a range of thresholds used in each cloud test. For example, the reflectance is very low in the M5 band (0.672  $\mu\text{m}$  bandpass) over densely vegetated surfaces and ocean surfaces outside sun glint regions. Therefore, the cloud confidences (given as a fraction between 0 and 1) for the original M5 Reflectance Test (Reed, 2002) were assigned according to criteria shown in Table 4, where M5 values of reflectance are given in percent. (The simplicity of this test was a major error source in VCM analyses and the test has been significantly enhanced, as will be shown in Section 4.3)

**Table 4 here.**

Cloud confidence is also assigned based upon a combination of results from multiple tests that exploit cloud and background signatures in VIIRS reflective and emissive bands, as shown in Figure 2. For example, in the original VIIRS cloud mask algorithms (Reed, 2002), if the outcome of either cloud test that exploits the solar energy (i.e. the M7/M5 Ratio or the M5 Reflectance Tests) is confidently cloudy, then the pixel is assigned this classification, as shown by “min” in Figure 2. Similarly, if the outcome of either the M15-M12 BTDR Test or the M12-M13 BTDR Test is confidently cloudy, the pixel is assigned this classification. Therefore, it is imperative that none of these cloud tests generate an unacceptable number of false alarms. The result of each individual cloud test is also produced as output for each pixel.

**Figure 2 here.**

Finally, the VCM algorithms produce a cloud top phase classification. Initially the approach used was based upon the NASA MODIS algorithms (Strabala et al., 1994; Menzel et al., 2002). However, a new technique that identifies overlap conditions, i.e. occurrence of ice clouds over water clouds in a single VIIRS pixel, has been developed through the NPOESS IPO (Pavolonis and Heidinger, 2004). This logic has been recently integrated into the VCM algorithms, which now produces seven cloud phase classifications including water, thin cirrus, thick cirrus, mixed phase, and overlap, along with clear, partly cloudy, and not executed.

### **3.0 TEST DATA SETS**

The performance of VCM algorithms has been established using two types of data sets: truth data sets used in the generation of global synthetic data and manual cloud analyses of MODIS granules using well-known procedures (Hutchison et al., 1995; Hutchison and Choe, 1996; Hutchison and Jackson, 2003). The test data used to determine VCM performance is now briefly highlighted.

### **3.1 GENERATION OF GLOBAL SYNTHETIC CLOUD DATA**

The global geophysical database, used to generate synthetic cloud data, has been discussed in the literature and is briefly highlighted here (Grano et al., 2004). The database contains 24 days of NCEP analyses, consisting of 2 days/month between July 2001 and June 2002, which provides an ensemble of over 6 million surface/atmosphere situations. From this data set, sub-sampling is used to create about 700,000 surface/atmosphere situations for performance verification.

Top of the atmosphere (TOA) VIIRS radiances are generated for the three NPOESS orbits, i.e. 1330, 1730, and 2130 ascending nodes, using the VIIRS swath and scan specifications illustrated in Figure 3 with various radiative transfer models such as MODTRAN (Berk et al., 1989). It has been shown that TOA radiances generated from a newly upgraded MODTRAN4.v4 using the 16-stream DISORT option along with user-defined ice and water cloud phase functions compares quite well, in most cases, with the more precise UCLA Line-by-Line Equivalent Model that employs the Adding-Doubling Method with 200-term expansions of the scattering phase functions (Ou et al, 2004).

These TOA radiances are then passed through the VIIRS sensor model, calibrated, and converted to engineering units, i.e. reflectances or equivalent blackbody (brightness) temperatures. The approach used to construct the geophysical database includes the following steps:

- Tropospheric data from the NCEP AVN-FNL are used to describe the state of the atmosphere and surface backgrounds. These data are assimilated by NWS and re-generated onto a uniform one-degree equal-angle lat/lon grid covering the globe. Atmospheric profiles of temperature, geo-potential height, relative humidity, cloud liquid water, ozone, and vector-winds are specified at up to 25 pressure levels, from 1000 mb to 10 mb. These data are generated four-times daily, at 00Z plus 6-hours.
- Stratospheric and climatologic data provided by the NCEP CIRA-86 and UARS reference atmospheres are used to extend key atmospheric profiles to higher altitudes (i.e., pressures less than 10mb).
- Cloud liquid water profiles contained in the NCEP tropospheric datasets, are converted to cloud parameters (i.e. cloud layers, cloud type, phase, top-height, base-height, optical thickness, and effective particle size) by the Cloud Scene Simulation Model (Cianciolo et al., 1996).
- Aerosols are extracted from the MODIS L3 8-Day Joint Aerosol/Water Vapor/Cloud Product (MOD08\_E3), which in turn is derived from the corresponding MODIS Level 3 daily dataset (MOD08\_D3).

- Surface elevation, material determination, and spectral albedos come from a high-resolution (30 arc-seconds) terrain database available through Photon Research Associates.

**Figure 3 here.**

### **3.1 VIIRS PROXY DATA BASED UPON MODIS GRANULES**

In addition, six MODIS granules were selected to quantify VCM performance. In these cases, truth consisted of a manual interpretation of the imagery using procedures described in the VIIRS Imagery Algorithm Theoretical Basis Document (Hutchison et al., 2002). These manual analyses are binary cloud maps generated with special software that allows a trained image analyst to identify clouds in a given channel by making all pixels cloudy that have values that exceed a user-defined threshold. Similarly, all pixels with values less than the threshold value remain cloud-free. Each scene typically needs to be segmented into many sub-regions to accurately delineate cloudy and cloud-free regions, especially for scenes of large geographic regions or highly heterogeneous conditions, since some cloud-free land surfaces may have pixel values similar to clouds in another part of the scene. In addition, manual analyses from multiple channels may be merged into a single, composite cloud, no cloud analysis.

Color composite images of the MODIS granules used to establish initial VCM performance, as discussed in Section 4.1, are shown in Panels (a) – (d) of Figure 4. Additional MODIS granules continue to be added to the VCM verification test data base

including those in Panels (e) and (f) of Figure 4, which are discussed further in Sections 4.2 and 4.3. These scenes include a variety of cloud fields observed over diverse atmospheric and surface conditions:

- Western Africa desert, with blowing sand, ocean, and various clouds shown in Figure 4, Panel A - and collected at 1210 UTC on August 1, 2001.
- Greenland with ice, vegetated land, bare soil, ocean and various clouds shown in Figure 4, Panel B - collected at 2240 UTC on July 15, 2001.
- Intermountain West USA with sparsely vegetated land and various clouds shown in Figure 4, Panel C - collected at 1750 UTC on February 1, 2002.
- Tropical Atlantic with vegetated land, ocean, and various clouds, shown in Figure 4, Panel D - collected at 1220 UTC on July 15, 2001.
- Gulfstream along US East Coast region with strong sunglint, ocean thermal gradients, various clouds, shown in Figure 4, Panel E – collected at 1600 UTC on June 1, 2001.
- Northwest China with desert, snow, blowing snow, mountains, various clouds shown in Figure 4, Panel F – collected at 0340 UTC on January 1, 2002.

**Figure 4 here.**

## **4.0 VIIRS CLOUD MASK ALGORITHM PERFORMANCE**

### **4.1 PRELIMINARY RESULTS**

Initial VCM results, based upon the analysis of global synthetic data, showed an overall error rate in the binary cloud mask of about 36% in the nearly 700,000 pixels of which

115,000 were cloudy. These results were stratified by solar illumination conditions, (e.g. daytime versus nighttime), surface backgrounds, and orbital nodes. For all pixels, false alarm rates (defined as the number of confidently cloud in the VCM but clear in the truth divided by the number of pixels) were over 44%, while leakage (defined as the number of confidently clear in the VCM but cloudy in the truth divided by the number of pixels) exceeded 18%. Over the ocean, the false alarm rate exceeded 30% in areas outside sun glint while the leakage rate was 28.5% within sun glint regions.

Through diagnostic analyses, it was found that several coding errors were made while translating the MODIS Cloud Mask Algorithm code into the VIIRS Cloud Mask Algorithm. After these coding errors were corrected, results were re-generated with the corrected algorithms, and stratified by NPOESS orbital node, as shown in Table 5.

**Table 5 here.**

Performance of the VCM algorithms, based upon the analysis of MODIS granules shown in Figure 4, was also found to be inadequate, as shown in Table 6. Error rates ranged between about 6-25% with false alarms being the primary cause for concern. A reanalysis of these scenes was completed after the coding errors, mentioned above, were corrected. In this case, the results are shown for land pixels only in Table 7. It is evident that the corrected algorithm reduced the number of false alarms but the rates continued to be too large, especially over the US Great Basin scene. While the false alarm rates in the Greenland scene are high, there are few land pixels in the scene to impact the overall

error rate. (As noted in Section 3.2, MODIS scenes shown in Panels (e) and (f) of Figure 4 were added to the verification test database after these initial results were obtained in March 2003.)

**Table 6 here.**

**Table 7 here.**

The corrected VCM algorithms produced more accurate results but performance remained grossly inadequate to meet NPOESS system requirements. Thus, the VCM algorithms were entered into a remediation program by Northrop Grumman Space Technology (NGST) in collaboration with staff from NOAA's National Satellite, Data, and Information Service (NESDIS), and the Aerospace Corporation. More recently, members of the University of Wisconsin Cooperative Institute for Meteorological Satellite Studies (CIMSS) became a partner in this collaboration. Results of those remediation activities are shown in the next sub-sections.

It is emphasized at this point that, while based upon the MODIS cloud mask algorithms, the VCM algorithms do not reflect the performance of the former. Due to differences between schedules for the VIIRS acquisition process and first launch of the NASA MODIS sensor, the VCM algorithms were based upon the 1997 version of the MODIS algorithms. On the other hand, these MODIS algorithms continued to mature after the launch of the NASA Earth Observing System Terra spacecraft in 2000 and a newer version of the MODIS Cloud Mask Algorithms has been released (Ackerman et al., 2002). At about the same time, the NGST NPOESS algorithm verification team identified

deficiencies in the original VCM algorithms and proposed enhancements to resolve them. The approaches selected differ from procedures used in the MODIS algorithms due to differences in MODIS and VIIRS sensor characteristics and the more rigorous VIIRS performance requirements established for the NPOESS system.

As stated previously, two major class problems were identified during initial VIIRS Cloud Mask Algorithm verification testing including an unacceptable leakage rate over ocean surfaces and an unacceptable false alarm rate over land surfaces. These problems believed to result from two primary sources which could readily be addressed. First, a failure to use a sea surface temperature field in the VCM algorithms contributed to leakage over ocean surfaces. Initially the use of an M15 (11  $\mu\text{m}$ ) test based upon a sea surface temperature database was proposed to correct this problem. In fact, a different solution was implemented, i.e. spatial tests that use 375 m VIIRS imagery channels, based upon CLAVR heritage (Heidinger, 2004). This enhancement will be discussed at length in Section 4.2. Secondly, false alarms over land surfaces resulted from the use of single-valued cloud tests, e.g. as shown in Table 4, with a static land surface data base that had an insufficient number of land classes, as shown in Figure 1. The proposed solution for this problem was to add additional land classes but the solution implemented uses a routinely updated vegetation index, again based upon CLAVR heritage (Heidinger, 2004) along with a new technique to vary the cloud detection thresholds with changes in vegetation index and scattering geometry, as will be shown in Section 4.3.

## **4.2 REDUCING LEAKAGE OVER OCEAN SURFACES**

VIIRS will provide high (375 m) resolution Imagery data in the 0.640, 0.865, 1.6, 3.74, and 11.45  $\mu\text{m}$  bandpasses, which are nested inside the moderate resolution (750 m) Radiometric channels. Therefore, it was decided that a straightforward approach to reduce leakage over ocean surface could be implemented in both daytime and nighttime conditions using spatial tests based upon Imagery channels. Thus, spatial tests with the I2 Channel (0.865  $\mu\text{m}$  band) and I4 Channel (3.74  $\mu\text{m}$  band) were implemented to detect water clouds during the daytime and nighttime conditions respectively while another spatial test, with the I5 Channel (11.45  $\mu\text{m}$  band), is used to detect cirrus. However, these spatial tests can only change the pixel cloud confidence from confidently clear or probably clear to either probably clear or probably cloudy. The maximum, minimum, and the mean are determined from the four imagery pixels that make up the radiometry pixel. If the difference between the maximum and minimum exceeds a threshold and the mean is larger (smaller) than the average of the reflectance (brightness temperature) maximum and minimum values, the moderate resolution pixel is classified at probably cloudy. If the difference between the maximum and minimum exceeds the threshold and the mean is smaller (larger) than the average of the reflectance (brightness temperature) maximum and minimum values, the moderate resolution pixel is classified at probably clear.

The concept of using a spatial test to detect cloudy pixels over all ocean conditions, including sun glint regions, was prototyped and results compared against a sub-set of the MODIS granules shown in Figure 4. The prototype uses the MODIS M13 band ( $\sim 0.667 \mu\text{m}$ ) since its 500 m resolution nests within the 1 km MODIS channels in a manner similar to that planned for use with the VIIRS Imagery and Radiometry bands in the

VCM algorithms. Spatial tests based upon the 1 km resolution 3.74  $\mu\text{m}$  and 11.45  $\mu\text{m}$  bands were also prototyped; however, results obtained from applying these tests are biased strongly toward false alarms, since a large area is effected by the tests, as shown in Figure 5. Once VIIRS Imagery data become available with the NPP launch, all spatial tests will be applied with the logic shown for the 500 m data in Figure 5.

**Figure 5 here.**

Results from the analysis of the MODIS scene shown in Figure 4(e) are given in Figure 6. The four panels, (a) – (d), show the manual truth cloud mask, the region of sun glint, the VCM cloud confidence, and the comparison between the cloud confidence and the truth cloud mask, respectively. In panel (d), under-clouding or leakage occurs when the cloud confidence of a pixel is classified as confidently clear or probably clear and the truth is cloudy. Over-clouding or false alarms occur when the cloud confidence of a pixel is classified as confidently cloudy or probably cloudy and the truth is clear. Areas of agreement result from pixels possessing the VCM clear labels and clear as truth or the VCM cloudy labels and cloud as truth or by being non-ocean. Much of the disagreement between the truth cloud mask and the VCM cloud confidence occurs within the confidence categories of probably clear and probably cloudy.

**Figure 6. here.**

Results from the analysis of the three scenes consisting primarily of ocean surfaces, both without (original VCM) and with (final VCM) the spatial tests, are presented in Table 8. These statistics clearly show that leakage is greatly reduced by the spatial test in every case, especially within sun glint regions and is within the NPOESS System Specification that calls for 99% accuracy, as shown in Table 1. False alarms and errors in the binary cloud mask continue to be larger than desirable but these numbers will be reduced after VIIRS data become available. These reductions will result from two reasons: first, the superior VIIRS spatial resolution (375 m at nadir growing to only 750 m at edge of a 3000 km scan) will produce fewer sub-pixel cloud situations compared to AVHRR (which grows from 1.1 to almost 6 km at edge of swath) and MODIS (which also experiences similar pixel growth across swath). Secondly, thresholds for the spatial cloud tests used in these analyses were taken from the CLAVR algorithms, i.e. optimized to detect clouds in AVHRR data. As the launch date for VIIRS approaches, these thresholds will be tuned for the VIIRS sensor, once instrument characterization is complete.

**Table 8 here.**

#### **4.3 REDUCING FALSE ALARMS OVER LAND SURFACES**

From Table 6, it was seen that false alarms were greatest in the US Great Basin scene. They are also large in the Greenland and West Africa scenes; however, in the former the number of pixels was extremely small and false alarms in the latter occurred only in the vicinity of heavy sand blowing over the ocean surface, which can be eliminated by adding a cloud-free restore test using the 0.412  $\mu\text{m}$  band as shown previously by using

this same band over land surfaces (Hutchison and Jackson, 2003). Therefore, attention turns to the MODIS scenes collected over the US Great Basin, shown in Panel (c), plus a new scene over NW China, shown in Panel (f) of Figure 4, which was selected based upon difficulties this region represents for heritage cloud mask algorithms. Results of individual cloud tests for these scenes best illustrate the second class problem found with the VCM algorithms, i.e. high false alarm rates associated with cloud detection tests as shown in Table 9 and Table 10.

**Table 9 here.**

**Table 10 here.**

It is evident from these tables that four cloud tests were generating false alarms; however, the cirrus solar (CIRSOL) test, which is based upon the 1.38  $\mu\text{m}$  bandpass, does not represent a concern at this time since improved performance with this band will result from the VIIRS hardware design, i.e. a 50% more narrow VIIRS bandpass compared to MODIS, along with smaller pixel size and growth. More concern centered on the other cloud tests, including.

- The M12 – M13 BTD Test produced the largest number of false alarms. It was subsequently found that this clouds test had been applied incorrectly. In reality, a cloud is indicated if this difference is greater than the threshold; but, the test was erroneously coded to classify a pixel as cloudy when this difference was less than the threshold value. The large number of false alarms was greatly reduced after the coding error was corrected.

- A large number of false alarms was also generated by the M15-M12 BTD test. Results from this cloud test were plotted for the entire global synthetic data set, shown in Figure 7, as a function of total precipitable water (TPW). It is seen that the original threshold midpoint of  $-14^{\circ}\text{C}$ , shown by the dashed line, falls in the cloudy pixels (red dots). It is also evident that better separation between cloudy and cloud-free pixels (blue dots) occurs at a threshold near  $-18^{\circ}\text{C}$  for most values of TPW greater than about 2 cm. After changing this threshold midpoint to its new value of  $-18^{\circ}\text{C}$ , results from re-testing showed a reduction in false alarms in the MODIS scene over the U.S. Great Basin from 53.89% to 4.8% as seen in Table 13 under without NDVI.
- The final large contributor to false alarms was the M5 reflectance test. While, in some cases, the false alarm rate for this test was less than that of the other tests already discussed, its solution is more complex. (Additionally, a similar M7 reflectance test was eliminated since it is redundant with and inferior to the M5 Reflectance Test.)

**Figure 7 here.**

As shown in Table 4, the M5 Reflectance Test was originally implemented with a constant threshold value that is applied to all land surface types shown in Figure 1, except snow. In reality, this test is most useful for densely vegetated surface where cloud-free M5 reflectances are small. As surfaces become more sparsely vegetated, reflectances in this band typically increase significantly, as shown in Figure 8, and cloud-free surfaces

can become indistinguishable from clouds. Unfortunately, the original VCM algorithms did not have sufficient land stratifications to compensate for global variations in land cover. In addition, the original cloud mask algorithm did not include a geographic database that changed with seasonal variations in vegetation. For example, Figure 9 illustrates the variations in global Normalized Difference Vegetation Index (NDVI) in composites for July and January which are due to seasonal oscillations in global precipitation patterns.

**Figure 8 here.**

**Figure 9 here.**

First, the VCM algorithms were modified to accept an NDVI field constructed from a daily-composite top-of-canopy (TOC) NDVI product. To assess the value of these fields on VCM performance, NDVI data were generated from the MODIS 17-day 0.65  $\mu\text{m}$  and 0.86  $\mu\text{m}$  surface reflectance composites. The NDVI field constructed for the NW China scene is shown in the left panel of Figure 10 along with the manually-generated cloud analysis which serves as truth for comparisons against VCM analyses.

**Figure 10 here.**

Next, the logic used in the M5 Reflectance Test was modified from that shown in Table 4 to that shown in Table 11, using procedures in the heritage CLAVR algorithms (Heidinger, 2004). Note that the thresholds are based upon an initial M5 (IM5) guess, used in the CLAVR algorithms and shown in Figure 11. However, this initial guess is

modified upward slightly allow the number of false alarms to be controlled once VIIRS data become available. For example, the highest threshold (M5\_Lo), representing a low confidence clear, will be the maximum of either the IM5 value after it is increased by 37.5% or 0.075. Similarly, the other two thresholds, i.e. M5\_Mid and M5\_Hi are designed to ensure that the thresholds for these tests remains below that used for M5\_Lo for all NDVI values. These thresholds were more significantly modified for use in the terminator orbit, as shown in Figure 12. The constant values used for scattering angles less than 80-degrees are considered placeholders until more accurate thresholds can be established. Reliable synthetic cloud data cannot be currently generated for the terminator orbit with MODTRAN; therefore, updates to these thresholds may await post-launch analysis of actual VIIRS data.

**Table 11 here.**

**Figure 11 here.**

**Figure 12 here.**

Finally, the VCM algorithms, with the addition of the NDVI field and algorithmic logic described above and without it, were executed on the MODIS granules. Differences between performance of the M5 Reflectance Test contained in the original VCM algorithms (without an NDVI field) and current VCM algorithms (with the NDVI fields) are shown for the NW China scene in Figure 13 and Figure 14 respectively while the results are summarized in Tables 12 and 13. It is seen that false alarms produced by the M5 Reflectance Test over land surfaces have been substantially reduce, i.e. from 60.9 %

to 6.9% in Table 12, by exploiting the NDVI data. (In addition, cloud tests that use the daytime 3.7 and 4.0  $\mu\text{m}$  bands, i.e. M12 and M13 respectively, are not used when NDVI falls below 0.2 which results in a negligible number of false alarms being produced by these tests.) Similar but less dramatic similar results are shown in Table 13.

**Table 12 here.**

**Table 13 here.**

**Figure 13 here.**

**Figure 14 here.**

Additional analyses were undertaken to examine reasons for continued false alarms and leakage with the M5 Reflectance Tests as shown in Tables 12 and 13. While not fully presented here due to space limitations, it was found that most of the leakage with this test occurs when NDVI values fall below 0.1 while false alarms occur at NDVI values closer to 0.3, which suggests that no single M5 reflectance threshold, based on NDVI, will be able to accurately classify all VIIRS pixels. Thus, a change toward another band is considered essential perhaps using a VIIRS M1 (0.412  $\mu\text{m}$ ) Reflectance Test. Evidence for this change is shown in Figure 15, which shows reflectance values for the MODIS 0.66  $\mu\text{m}$  band (left panel) and MODIS 0.412  $\mu\text{m}$  band (right panel) as a function of NDVI for pixels classified by a prototype of the VCM as cloudy (red) and cloudy-free (green) pixels. This MODIS granule contained the western Sahel region of Africa on April 4, 2003. The reduced area of overlap in the 0.412  $\mu\text{m}$  band compared to the substantial overlap at 0.66  $\mu\text{m}$  suggests that fewer false alarms and improved cloud

detection will result by switching from an M5 Reflectance Test to an M1 Reflectance Test at low NDVI values.

## **5. FUTURE WORK**

Two class problems were identified in verification testing of the VIIRS Cloud Mask Algorithms. One resulted in a failure to detect cloud-contaminated pixels over ocean surfaces, both within and outside sun glint regions. The other was a gross over-clouding of land surfaces where clouds are not present. Together, these deficiencies produced cloud analyses that far exceeded error rates contained in the NPOESS System Specification.

Solutions to these cloud classification problems have been implemented and VCM expected performance established using MODIS granules. The first approach involves the use of spatial tests over ocean surfaces using the relatively high resolution (375 m) VIIRS visible and infrared imagery channels that degrade to no more than 750 m at edge of swath. The latter problem is resolved through the exploitation of a background NDVI field which allows thresholds associated with the M5 Reflectance Test to vary with NDVI value and scattering geometry. In addition, the NDVI field is used to establish lower limits for other tests that use brightness temperature differences of bands viewing the short-wave IR region, i.e. 3.7  $\mu\text{m}$  and 4.0  $\mu\text{m}$  bands. Finally, evidence suggests that further reductions can be achieved in both leakage and false alarm error rates over land

surfaces by switching from the M5 Reflectance Test to one using the M1 (0.412  $\mu\text{m}$ ) band at very low NDVI values.

The task of meeting NPOESS system specification for VCM performance is daunting. Routinely achieving performance measures of 99% accuracy in the daytime product over ocean surfaces outside sun glint regions or 93% accuracy over land surfaces requires that every VCM cloud test perform correctly. Additional enhancements to the VCM have been identified and are planned to implementation, including:

- Using a variable threshold technique with the M9 (1.38)  $\mu\text{m}$  channel for improved cloud screening during daytime conditions (Roskovensky and Liou, 2003). Tables 9 and 10 shows that this test is now the largest source of error in the daytime VCM algorithm. However, implementation of this enhancement and other corrections may await work on VIIRS sensor characterization. Other actions awaiting sensor characterization are:
  - Update to thresholds for spatial tests based upon VIIRS imagery channels, as sensor becomes more fully characterized
  - Update to M5 and M1 thresholds for VIIRS channels, as sensor becomes more fully characterized
- Implementing an aerosol restoration procedure to ensure aerosols are not classified as confident cloudy pixels. For example, it may suffice to use the dual-gain M1 (0.412)  $\mu\text{m}$  channel over ocean regions adjacent to deserts to restore heavy aerosols into cloud-free conditions (Hutchison and Jackson,

2003). Over land, another approach is being evaluated using this band with the M11 (2.25)  $\mu\text{m}$  channel (Ou et al, in press).

- Replacing the current VCM ecosystem map with a VIIRS Quarterly Surface Type IP and EOS Land/Sea Mask. (The VCM currently uses an outdated and static USGS (Olson) Ecosystem map that is considered inadequate.)
- Using the NDVI field with the M7/M5 ratio test and M5 reflectance test to resolve misclassifications shown in Table 13 that are associated with cloud-free, mixed pixels that contain both land and water surfaces which have spectral signatures similar to clouds (Hutchison and Hardy, 1995), and
- Using the NDVI field with the I1 (0.640  $\mu\text{m}$ ) imagery channel spatial test for enhanced cumulus cloud detection over land and coastal surfaces.
- Developing a thin cirrus flag to replace a spare bit in the VCM output.
- Replacing the VCM fire detection logic with the VIIRS active fire mask product.

Prior to the launch of the first VIIRS on the NASA NPP mission in 2006, all cloud thresholds will be re-evaluated using a new sensor model based upon more completed sensor characterization analyses. With the engineering development unit (EDU) model scheduled for delivery to NGST in mid- 2005 and flight vehicle 1 (FV1) system delivery scheduled for six month later, these updated sensor models will be used along with new simulations based upon recent enhancements to MODTRAN to re-generate global synthetic data as discussed in Section 3. With the launch of the NPP, these thresholds will be fine-tuned to obtain the highest quality analyses from VIIRS data collected on-orbit.

## **6. CONCLUSIONS**

Highly accurate automated cloud analyses are essential for the production of operational environmental data products from meteorological satellite data collected by the NPOESS system for a variety of users in the U.S. and around the world. The VIIRS Cloud Mask Algorithms were based upon sound technology developed by the NASA MODIS Cloud Mask team prior to the launch of the first MODIS sensor on the EOS Terra satellite and the latter algorithms continued to be enhanced after on-orbit data became available.

Once the inadequate performance of the original VIIRS Cloud Mask Algorithms became evident, a collaboration was established between cloud experts at Northrop Grumman, NOAA NESDIS, CIMSS, and the Aerospace Corporation to ensure that these algorithms would produce high quality analyses for a variety of applications, including retrieval of land and ocean surface characteristics, atmospheric aerosols, and cloud properties (cloud top phase, cloud optical properties, cloud top parameters, cloud base heights). The results from this collaboration merged the most useful technology available from research and operational users into an enhanced version of the VIIRS Cloud Mask Algorithms that are now expected to satisfy this wide range of user requirements.

## **7. ACKNOWLEDGMENTS**

We acknowledge the support and encouragement received from leadership at NGST, the NPOESS IPO, NOAA NESDIS, CIMSS, and The Aerospace Corporation.

## 8. REFERENCES

Ackerman, S. Strabala, K., Menzel, P., Frey, R., Moeller, C., Gumley, L., Baum, B., Schaaf, C., and G. Riggs, 1997: Discriminating clear-sky from cloud with MODIS, NASA Algorithm Theoretical Basis Document (MOD35), pp 95.

Ackerman, S. A., Strabala, K. I., Menzel, W. P., Frey, R. A., Moeller, C. C. and L. E. Gumley, 1998: Discriminating clear sky from clouds with MODIS, J. Geophys. Res., **103** (D24), 32,141-32,156.

Ackerman, S., Strabala, K., Menzel, P., Frey, R., Moeller, C., Gumley, L., Baum, B., Seaman, S. W. and H. Zhong, 2002: Discriminating Clear-Sky from Cloud with MODIS Algorithm Theoretical Basis Document, MODIS ATBD Reference Number ATBD-MOD-06, pp 115.

Berk, A., Bernstein, L. S., and D. C. Robertson, 1989: MODTRAN: A Moderate Resolution Model for LOWTRAN 7, A. F. Geophysics Laboratory Technical Report, GL-TR-89-0122, Hanscom Air Force Base, MA, pp 38.

Formatted: English (U.S.)

Cianciolo, M.E., Raffensberger, M.E., Schmidt, E.O., and J.R. Stearns, 1996: Atmospheric scene simulation modeling and visualization. Phillips Laboratory (PL) Technical Report (TR), PL-TR-96-2079, Hanscom Air Force Base, MA, pp 110.

Formatted: English (U.S.)

Grano, V., Scalione, T., Emch, P., Agravante, H., Hauss, B., Jackson, J., Mills, S., Samec, T. and M. Shoucri, 2004: End-to-end performance assessment of the National Polar-orbiting Operational Environmental Satellites System Environmental Data Records, Weather and Environmental Satellites, Proc. of SPIE, **5549**, 53-59.

Gustafson, G. B., Isaacs, R. G., d'Entremont, R. P., Sparrow, J. M., Hamill, R. M., Johnson, D. W., Sarkisian, C. P., Peduzzi, D. C., Pearson, B. T., Jakabhazy, V. D., Belfiore, J. S., and A. S. Lisa, 1994: Support of environmental requirements for cloud analyses and archive (SERCAA): algorithm descriptions, US Air Force Phillips Laboratory Tech. Report, 94-2114, Hanscom Air Force Base, MA, pp 100.

Heidinger, A., 2004: CLAVR Cloud Mask Algorithm Theoretical Basis Document, NOAA NESDIS Office of Research and Applications, pp 68.

Formatted: English (U.S.)

Hutchison, K. D., Hardy, K. R. and G. C. Gao, 1995: "Improved Detection of Optically-Thin Cirrus Clouds in Nighttime Multispectral Meteorological Satellite Imagery using Total Integrated Water Vapor Information," *Journal of Applied Meteorology*, **34**, 1161-1168.

Hutchison, K. D. and N. J. Choe, 1996: "Application of 1.38 Micron Imagery for Thin Cirrus Detection in Daytime Imagery Collected Over Land Surfaces," *International Journal of Remote Sensing*, **17**, 3325-3342.

Hutchison, K. D. and K. Hardy, 1995: Threshold functions for automated cloud analyses of global meteorological satellite imagery, *International Journal of Remote Sensing*, **16**, 3665-3680.

Hutchison, K. D. and J. M. Jackson, 2003: Cloud detection over desert regions using the 412 nanometer MODIS channel, *Geophysical Research Letters*, **30**, doi:10.1029/2003GL018446.

Hutchison, K. Jensen, K. and S. Miller, 2002, , VIIRS Imagery Algorithm Theoretical Basis Document, Appendix A – User's Guide for VIIRS Cloud Imagery Products, pp. 157.

Kriebel, K. T., Gesell, G., Kaestner, M. and H. Mannstein, 2003: The cloud analysis tool APOLLO: Improvements and validations, *Journal of Remote Sensing*, **24**, 2389-2408.

Liu Y. H., Key J. R., Frey R. A., Ackerman S. A., and W. P. Menzel, 2004: Nighttime polar cloud detection with MODIS, *Remote Sensing of Environment*, **92**, 181-194.

Menzel W. P., Baum, B. A., Strabala, K. I. and R. A. Frey, 2002: Cloud Top Properties and Cloud Phase Algorithm Theoretical Basis Document, MODIS ATBD Reference Number: ATBD-MOD-04, pp 61.

Formatted: English (U.S.)

Ou, S. C., Liou, K. N., Takano, Y. , Wong, E., Hutchison, K., and T. Samec, 2004: Comparison of the UCLA-LBLE Radiative Transfer Model and MODTRAN for Accuracy Assessment of the NPOESS-VIIRS Cloud Optical Property Algorithms, *Weather and Environmental Satellites*, *Proc. of SPIE*, **5549**, 80-89.

Pavolisin, M. J. and A. K. Heidinger, 2004: Daytime cloud overlap detection from AVHRR and VIIRS, *Journal of Applied Meteorology*, **43**, 762-778

Reed, B., 2002: VIIRS Cloud Mask (VCM) Algorithm Theoretical Basis Document for the Visible/Infrared Imager/Radiometer Suite, Version 5, Revision 2, pp 33.

Roskovensky J. K. and K-N Liou, 2003 Detection of thin cirrus using a combination of 1.38- $\mu\text{m}$  reflectance and window brightness temperature difference, *J. Geophys. Res.*, **108(D18)**, 4570, doi:10.1029/2002JD003346.

Saunders, R. W. and K. T. Kriebel, 1988: An improved method for detecting clear sky and cloudy radiances from AVHRR data, *International Journal of Remote Sensing*, **9**, 123-150.

Stowe et al., 1999 Scientific basis and initial evaluation of the CLAVR-1 global clear cloud classification algorithm for the advanced very high resolution radiometer, *Journal of Atmospheric and Oceanic Technology*, **16**, 656-681.

Strabala K. I., Ackerman, S. A., and W. P. Menzel, 1994: Cloud properties inferred from 8-12  $\mu\text{m}$  data, *Journal of Applied Meteorology*, **33**, 212-229.

### **Table Captions**

Table 1. Performance requirements for the VIIRS cloud mask algorithms as shown in the NPOESS System Specification.

Table 2. Comparisons between VIIRS channels used for cloud detection and those of heritage sensors.

Table 3. Cloud tests used in the VIIRS Daytime Cloud Mask Algorithm as a function of surface type.

Table 4. Classification of cloud confidence for M5 Reflectance Test in original VIIRS Cloud Mask (Reed, 2002).

Table 5. VIIRS Cloud Mask Algorithm performance for the analysis of global synthetic data.

Table 6. Initial VIIRS Cloud Mask Algorithm performance of MODIS proxy data.

Table 7. VIIRS Cloud Mask Algorithm performance for the analysis of MODIS scenes in Panels A – D of Figure 4.

Table 8. Results from the analysis of MODIS data in and outside sunglint regions with and without spatial tests.

Table 9. Performance of individual cloud tests used in the VCM analysis of the MODIS scene containing the U.S. Great Basin and shown in Panel C of Figure 4

Table 10. Performance of individual cloud tests used in the VCM analysis of the MODIS scene containing the NW China and shown in Panel F of Figure 4

Table 11. Cloud confidence definitions for M5 Reflectance Test in current VCM algorithm.

Table 12. VCM performance with and without NDVI for MODIS Scene A2002\_001\_0340 (NW China).

Table 13. VCM performance with and without NDVI for MODIS Scene A2002\_032\_1750 (US Great Basin).

**Table 1. Performance requirements for the VIIRS cloud mask algorithms as shown in the NPOESS System Specification.**

Paragraph Number	Solar Conditions/ Cloud Optical Thickness	NPOESS System Requirement
40.4.2-17a	1. Day, Ocean, OD = 0.5 or Less	92%
40.4.2-17b	2. Day, Ocean, OD > 0.5	99%
40.4.2-17c	3. Day, Land, OD = 1 or Less	85%
40.4.2-17d	4. Day, Land, OD > 1	93%
40.4.2-17e	5. Night, Ocean, OD = 0.5 or Less	90%
40.4.2-17f	6. Night, Ocean, OD > 0.5	96%
40.4.2-17g	7. Night, Land, OD = 1 or Less	85%
40.4.2-17h	8. Night, Land, OD > 1	90%
40.4.2-18	p. Degraded Conditions: sun glint area	Night Performance
40.4.2-19	q. Exclusion Conditions: Aerosol optical thickness > 1.0	

**Table 2. Comparisons between VIIRS channels used for cloud detection and those of heritage sensors.**

<b>VIIRS Channel</b>	<b>Band Center and Width (<math>\mu\text{m}</math>)</b>	<b>Heritage Sensor</b>	<b>VIIRS Enhancement</b>	<b>Value to VIIRS Cloud Mask Algorithms</b>
M1	0.412/0.020	MODIS Channel 8 SeaWiFS Channel 1	Dual Gain	Will not saturate in presence of clouds
I1 M5	0.640/0.080 0.672/0.020	MODIS Channel 1 MODIS Channel 13 AVHRR Channel 1 OLS LF	More accurately calibrated compare to AVHRR/OLS	Calibration provides more accurate analyses
I2 M7	0.865/0.039 0.865/0.039	MODIS Channel 2 MODIS Channel 16 AVHRR Channel 2	More accurately calibrated compare to AVHRR/OLS with more narrow bandpasses than AVHRR	Calibration provides more accurate analyses and narrow bandpasses reduce atmospheric attenuation due to water vapor
M9	1.378/0.015	MODIS Channel 26	Bandpass 50% more narrow	Reduces surface contamination
I3 M10	1.610/0.060 1.610/0.060	MODIS Channel 6 AVHRR Channel 3A	375 m in I3	Provides more accurate snow mask
I4 M12	3.740/0.380 3.700/0.180	MODIS Channel 20 AVHRR Channel 3B	375 m in I4	Reduces impacts from sub-pixel cloud
M13	4.050/0.155	MODIS Channel 23	750 m	Reduces impacts from sub-pixel cloud
M14	8.550/0.300	MODIS Channel 29	750 m	Reduces impacts from sub-pixel cloud
M15	10.763/1.00	MODIS Channel 31 AVHRR Channel 4	750 m	Reduces impacts from sub-pixel cloud
I5	11.450/1.90	OLS TF	Highly Calibrated 375 m in I5	Reduced impacts from sub-pixel cloud
M16	12.013/0.95	MODIS Channel 32 AVHRR Channel 5	750 m	Reduced impacts from sub-pixel cloud
DNB	0.7/0.4	OLS DNB	Accurately calibrated	Not used currently

Formatted: French (France)

**Table 3. Cloud tests used in the VIIRS Daytime Cloud Mask Algorithm as a function of surface type.**

<b>Cloud Tests</b>	<b>Water</b>	<b>Land</b>	<b>Desert</b>	<b>Coast</b>	<b>Snow</b>
1. M9 (1.38 $\mu\text{m}$ ) Reflectance Test	X	X	X	X	X
2. M15-M16 (10.76 – 12.01 $\mu\text{m}$ ) Brightness Temperature Difference (BTD)	X	X	X	X	
3. M15 (10.8 $\mu\text{m}$ ) Brightness Temperature (BT) Test	X				
4. M12-M16 (3.70–10.76 $\mu\text{m}$ ) BTD Test					
5. Tri-Spectral M14, M15, M16 ( 8.55, 10.76, 12.01 $\mu\text{m}$ ) BTD Test	X				
6. M15-M12 (10.76-3.70 $\mu\text{m}$ ) BTD Test	X (if no sun glint)	X	X (if Lat > 60° or < - 60°)	X (if no sun glint)	X
7. M12-M13 (3.70-4.05 $\mu\text{m}$ ) BTD Test	X (if –60° < Lat < 60°)	X (if –60° < Lat < 60°)	X	X	X (if –60° < Lat < 60°)
8. M5 (0.672 $\mu\text{m}$ ) Reflectance Test		X		X	
9. M7 (0.865 $\mu\text{m}$ ) Reflectance Test	X				
10. M7/M5 (0.865 / 0.672 $\mu\text{m}$ ) Reflectance Ratio Test	X	X			
11. M1 (0.412 $\mu\text{m}$ ) Reflectance Test			X		
12. I4 (3.74 $\mu\text{m}$ ) Spatial Test					
13. I5 (11.45 $\mu\text{m}$ ) Spatial Test	X				
14. I2 (0.865 $\mu\text{m}$ ) Reflectance Test	X				

**Table 4. Classification of cloud confidence for M5 Reflectance Test in original VIIRS Cloud Mask (Reed, 2002).**

<b>VIIRS M5 Reflectance Test</b>	<b>Cloud Detection Threshold (percent)</b>	<b>VIIRS Cloud Confidence</b>	<b>Remarks</b>
M5 equals or greater	18	Confidently Cloudy 0	Highest Threshold
14 < M5 < 18		Probably Cloudy Linearly interpolated between 0 and 0.5	
M5	14	0.5	Midpoint Threshold
10 < M5 < 14		Probably Clear Linearly interpolated between 0.5 and 1	
M5 equals or less than	10	Confidently Clear 1	Lowest Threshold

**Table 5. VIIRS Cloud Mask Algorithm performance for the analysis of global synthetic data.**

<b>Global Simulation Data</b>	<b>Original Algorithms Error Rate (Nighttime Water Clouds)</b>	<b>Corrected Algorithms Error Rate (Nighttime Water Clouds)</b>	<b>Original Algorithms Error Rate (All Conditions)</b>	<b>Corrected Algorithms Error Rate (All Conditions)</b>
<b>1330 Orbit</b>	65%	7%	36%	19%
<b>1730 Orbit</b>	65%	7%	45%	25%
<b>2130 Orbit</b>	66%	6%	37%	19%

**Table 6. Initial VIIRS Cloud Mask Algorithm performance of MODIS proxy data.**

<b>Scene 2002.032.1750 (US Great Basin</b>	<b>Error Rate</b>	<b>Leakage</b>	<b>False Alarm</b>
All Pixels	25.1%	1.37%	57.6%
<b>Scene 2001.213.1210 (West Africa)</b>			
All Pixels	25.2%	31.3%	22.9%
<b>Scene 2001.196.2240 (Greenland)</b>			
All Pixels	11.1%	2.4%	25.0%
<b>Scene 2001.213.1220 (Amazon Coast)</b>			
All Pixels	6.3%	9.0%	2.6%

**Table 7. VIIRS Cloud Mask Algorithm performance for the analysis of MODIS scenes in Panels A – D of Figure 4.**

<b>Scene 2001.213.1220 (Amazon Coast)</b>	<b>Error Rate</b>	<b>Leakage</b>	<b>False Alarm</b>
Land Pixels – Original algorithms	7.0%	03.3%	12.2%
Land Pixels – Corrected algorithms	7.0%	11.9%	0.0%
<b>Scene 2002.032.1750 (US Great Basin)</b>			
Land Pixels – Original algorithms	14.9%	2.1%	36.1%
Land Pixels – Corrected algorithms	8.2%	4.8%	13.7%
<b>Scene 2001.213.1210 (West Africa)</b>			
Land Pixels – Original algorithms	42.9%	7.0%	49.3%
Land Pixels – Corrected algorithms	31.1%	11.3%	34.5%
<b>Scene 2001.196.2240 (Greenland)</b>			
Land Pixels – Original algorithms	12.4%	0.0%	98.7%
Land Pixels – Corrected algorithms	12.4%	0.0%	98.9%

**Table 8. Results from the analysis of MODIS data in and outside sun glint regions with and without spatial tests.**

	<b>Binary Cloud Mask Error Rate Without (With) Spatial Tests</b>	<b>Leakage Rate Without (With) Spatial Tests</b>	<b>False Alarm Rate Without (With) Spatial Tests</b>
<b>Scene</b>			
<b>20012131210 (All Pixels)</b>	0.252 (0.1177)	0.313 (0.0003)	0.229 (0.053)
<b>Water Day Sun     Glint</b>	0.137 (0.0998)	0.519 (0.0006)	0.021 (0.0012)
<b>Water Day No Sun     Glint</b>	0.538 (0.1356)	0.033 (0.0000)	0.659 (0.105)
<b>Scene</b>			
<b>20012131210 (All Pixels)</b>	0.0626 (0.1287)	0.0904 (0.0118)	0.0260 (0.0094)
<b>Water Day Sun     Glint</b>	0.1104 (0.1771)	0.1974 (0.0122)	0.0001 (0.0000)
<b>Water Day No Sun     Glint</b>	0.0362 (0.0943)	0.0360 (0.0116)	0.0365 (0.0161)
<b>Scene</b>			
<b>20012131210 (All Pixels)</b>	0.1109 (0.1711)	0.1793 (0.0064)	0.0744 (0.0467)
<b>Water Day Sun     Glint</b>	0.1032 (0.1976)	0.2991 (0.0083)	0.0341 (0.0240)
<b>Water Day No Sun     Glint</b>	0.1253 (0.1218)	0.0656 (0.0028)	0.1878 (0.0891)

**Table 9. Performance of individual cloud tests used in the VCM analysis of the MODIS scene containing the U.S. Great Basin and shown in Panel C of Figure 4**

	Total Pixels	Cloudy Pixels	Clear Pixels	Detected	False Alarms	Detection Rate	False Alarm Rate
CIRSOL	623449	387428	236021	233868	20724	0.603642	0.087806
CIRIR	623449	387428	236021	186371	6184	0.481047	0.026201
M15M12DIF	623449	387428	236021	369718	127194	0.954288	0.538910
M12M13DIF	623449	387428	236021	186161	229855	0.480505	0.973875
M5REFL	623449	387428	236021	314639	37856	0.812123	0.160393
M7REFL	623449	387428	236021	0	0	0.000000	0.000000
M7M5RATIO	623449	387428	236021	245673	2826	0.634113	0.011974

**Table 10. Performance of individual cloud tests used in the VCM analysis of the MODIS scene containing the NW China and shown in Panel F of Figure 4.**

	Total Pixels	Cloudy Pixels	Clear Pixels	Detected	False Alarms	Detection Rate	False Alarm Rate
CIRSOL	1595279	458339	1136940	437605	141264	0.954763	0.124249
CIRIR	1595279	458339	1136940	211619	19766	0.461708	0.017385
IRTHESH	1595279	458339	1136940	0	0	0.000000	0.000000
M12M16HICLD	1595279	458339	1136940	0	0	0.000000	0.000000
TRISPEC	1595279	458339	1136940	0	0	0.000000	0.000000
M15M12DIF	1595279	458339	1136940	200907	203503	0.438337	0.178992
M12M13DIF	1595279	458339	1136940	220076	271128	0.480160	0.238472
M3REFL	1595279	458339	1136940	450696	689477	0.983325	0.606432
M7REFL	1595279	458339	1136940	0	0	0.000000	0.000000
M7M5RATIO	1595279	458339	1136940	389644	400927	0.850122	0.352637

**Table 11. Cloud confidence definitions for M5 Reflectance Test in current VCM algorithm that uses an NDVI field to select threshold values.**

VIIRS M5 Reflectance Test	Cloud Detection Threshold (percent)	VIIRS Cloud Confidence	Remarks
M5 equals or greater than (M5_Lo)	$M5\_Lo = IM5 + \text{MAX}(0.375 * IM5, 0.075)$	Confidently Cloudy 0	Highest Threshold
M5_Mid < M5 < M5_Lo		Probably Cloudy Linearly interpolated between 0 and 0.5	
M5_Mid	$M5\_Mid = IM5 + \text{MAX}(0.25 * IM5, 0.05)$	0.5	Midpoint Threshold
M5_Hi < M5 < M5_Mid		Probably Clear Linearly interpolated between 0.5 and 1	
M5 equals or less (M5_Hi)	$M5\_Hi = IM5 * + \text{Max}(0.125 * IM5, 0.025)$	Confidently Clear 1	Lowest Threshold

Formatted: German (Germany)

Formatted: German (Germany)

Formatted: German (Germany)

**Table 12. VCM performance with and without NDVI for MODIS Scene A2002\_001\_0340 (NW China).**

No NDVI	Land/Day	Clear	Cloudy	No.detected	No. False Alarms	Detection Rate	False Alarm rate
RM5	1595801	1142819	452982	444105	696068	0.9804	0.6091
BT15-BT12	1595801	1142819	452982	195661	208749	0.4319	0.1827
BT12-BT13	1595801	1142819	452982	215427	275777	0.4756	0.2413
With NDVI	Land/Day	Clear	Cloudy	No.detected	No. False Alarms	Detection Rate	False Alarm rate
RM5	1595801	1142819	452982	243926	79359	0.5385	0.0694
BT15-BT12	1595801	1142819	452982	44672	6281	0.0986	0.0055
BT12-BT13	1595801	1142819	452982	45876	9862	0.1013	0.0086

**Table 13. VCM performance with and without NDVI for MODIS Scene A2002\_032\_1750 (US Great Basin).**

No NDVI	Land/Day	Clear	Cloudy	No.detected	No. False Alarms	Detection Rate	False Alarm rate
RM5	1037241	565097	472144	363468	56180	0.7698	0.0994
BT15-BT12	1037241	565097	472144	394685	27250	0.8359	0.0482
BT12-BT13	1037241	565097	472144	249785	13177	0.529	0.0233
With NDVI	Land/Day	Clear	Cloudy	No.detected	No. False Alarms	Detection Rate	False Alarm rate
RM5	1037241	565097	472144	357608	40751	0.7574	0.0721
BT15-BT12	1037241	565097	472144	350369	11512	0.7421	0.0204
BT12-BT13	1037241	565097	472144	232184	6802	0.4918	0.012

### Figure Captions

Figure 1. Architecture of the VIIRS Cloud Mask Algorithm for the analysis of data collected in daytime conditions.

Figure 2. Architecture of cloud tests used to make cloudy confidences in the VIIRS Daytime Cloud Mask Algorithm.

Figure 3. Process of point sampling for global datasets.

Figure 4. MODIS granules used to assess performance of the VIIRS Daytime Cloud Mask Algorithm. (Note: some clouds may be indiscernible in the color composites.)

Figure 5. Pre-Launch Implementation of VIIRS Spatial Tests for Cloud Detection over Ocean Surfaces in MODIS Data.

Figure 6. Performance of the VIIRS Automated Cloud Analysis for the MODIS scene in shown Figure 4(e) using a spatial test based upon 0.865 $\mu$ m imagery channel. Manual analysis of clouds in MODIS scene in shown Figure 4(e) based upon human interpretation of imagery in Panel (a) with sun glint region shown in Panel (b). Automated cloud analysis in Panel © of MODIS scene in shown Figure 4(e) along with differences comparison with manual analysis from Panel (a) shown in Panel (d).

Figure 7. Observed B15-B12 BTD values found in the global synthetic data set for cloudy (red) and cloud-free (blue) pixels as a function of total precipitable water (TPW).

Figure 8. Spectral signatures of cloud particles and surface backgrounds in 0.3 - 1.0 micron range. (Key: Reflectivities: vegetated land = green, ocean = dark blue, snow = white, bare soil or sand = yellow., solar illumination = gold and atmospheric transmission = black. VIIRS bands blue, solid turquoise = index of refraction for water droplets, and dashed turquoise = index of refraction for ice.)

Figure 9. Typical changes in global NDVI fields during (a) January and (b) July due to variations in seasonal precipitation patterns (Heidinger, 2004).

Figure 10. NDVI field used in the of MODIS Scene A2002\_001\_0340 (left) along with manually generated cloud analyses used as truth in comparisons with VCM analyses (right)..

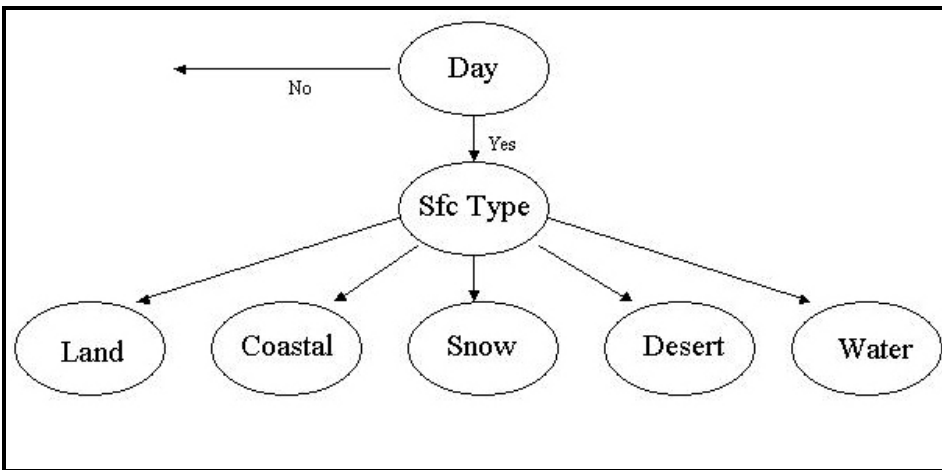
Figure 11. Logic for thresholds used with M5 Reflectance Test employs a 3-degree polynomial fit to curves shown for 10 NDVI bins that range from NDVI of  $-0.05$  through  $0.35$ , after CLAVR.

Figure 12. Logic for thresholds used with M5 Reflectance Test within the Daytime VCM algorithm allows the test to be evaluated with data collected in the terminator orbit.

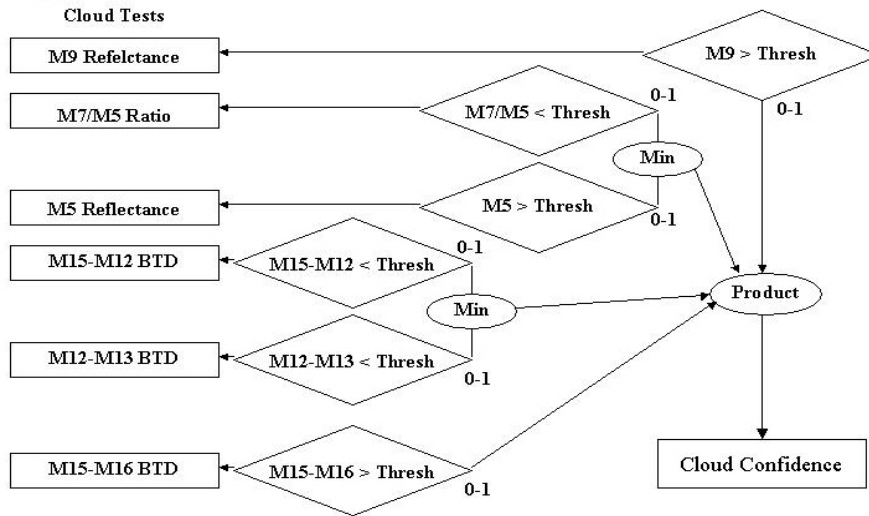
Figure 13. Cloud confidence (left) based upon the original VCM algorithm along with results of the M5 Reflectance Test (right). No NDVI data base was used in this analysis and the VCM used M5 Reflectance Test thresholds shown in Table 4.)

Figure 14. Cloud confidence (left) based upon the current VCM algorithm along with results of the M5 Reflectance Test (right). The NDVI data base shown in Figure 12 was used in this analysis along with M5 Reflectance Test thresholds shown in Table 11.

Figure 15. Reflectance in the M5 band (left) and M1 band (right) for pixels classified as cloud-free (green) and cloudy (red) by the MODIS cloud mask algorithms.



**Figure 1. Architecture of the VIIRS Cloud Mask Algorithm for the analysis of data collected in daytime conditions.**



**Figure 2. Architecture of cloud tests used to make cloudy confidences in the VIIRS Daytime Cloud Mask Algorithm.**

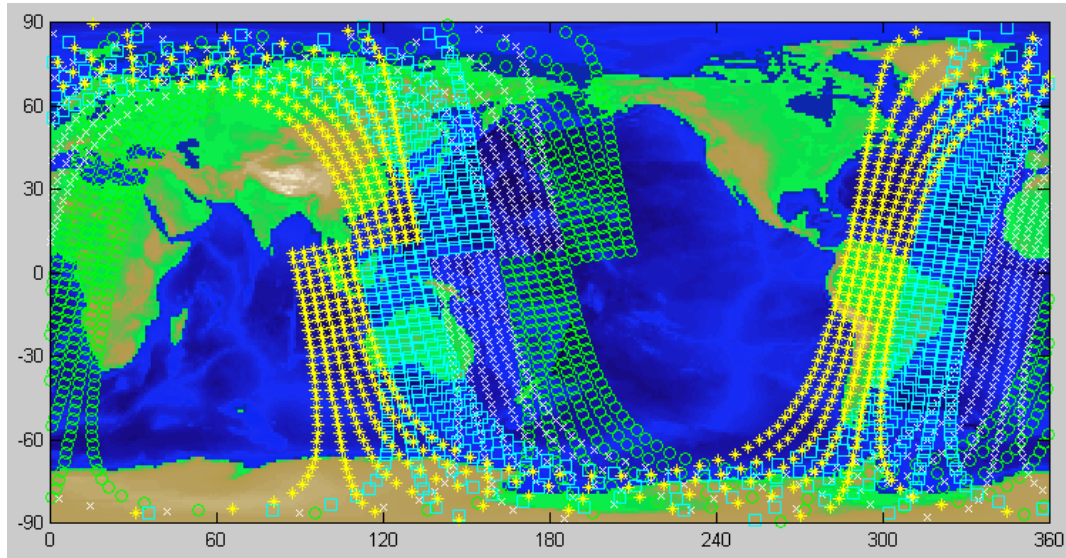
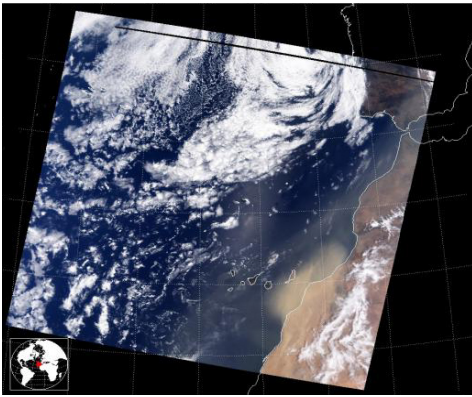
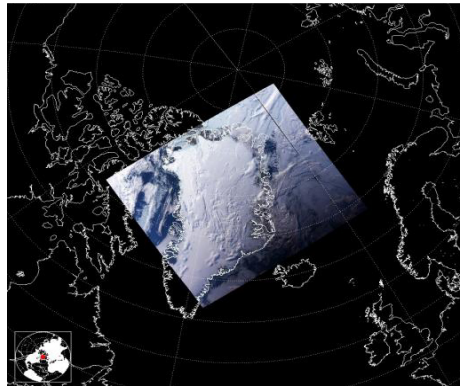


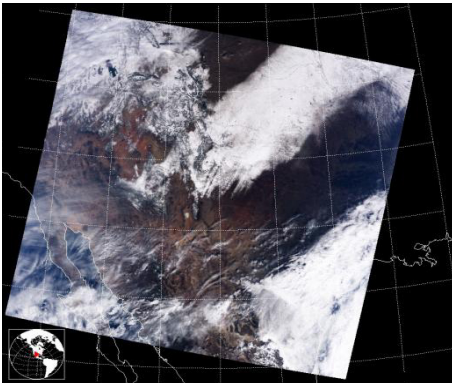
**Figure 3. Process of point sampling for global datasets.**



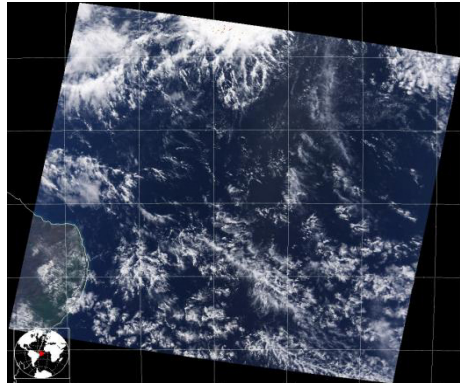
MODIS A2001.213.1210 (West Africa)



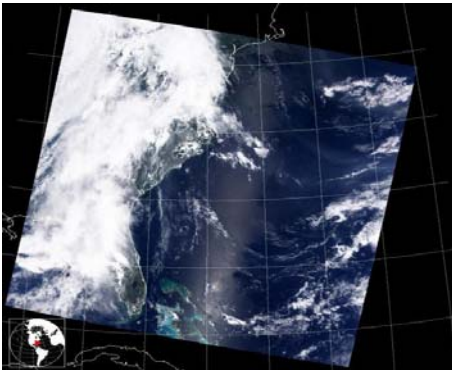
MODIS A2001.196.2240 (Greenland)



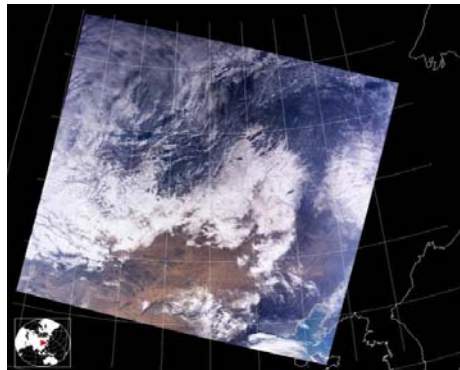
MODIS A2002.032.1750 (US Great Basin)



MODIS A2001.213.1220 (Amazon Coast)

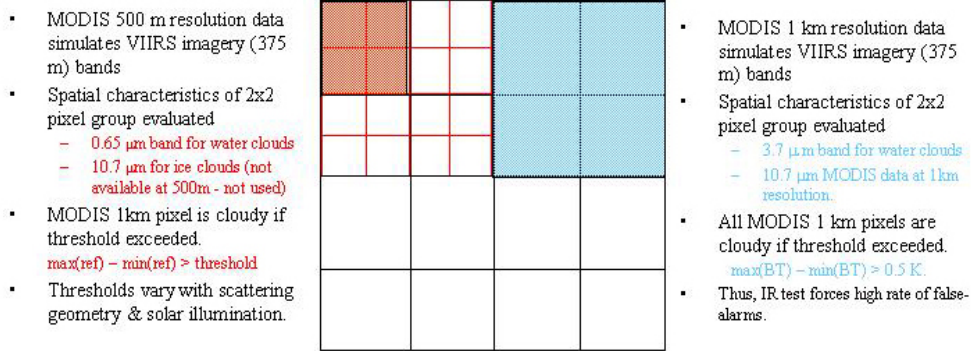


MODIS A2001.152.1600 (US East Coast)

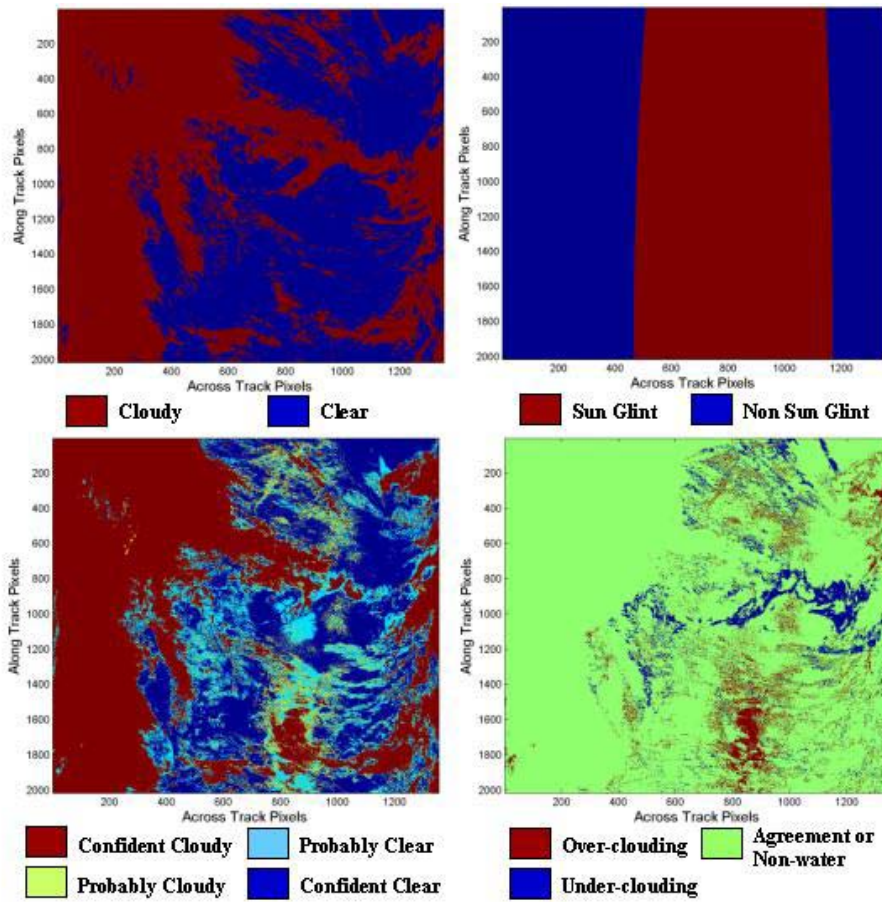


MODIS A2002.001.0340 (NW China)

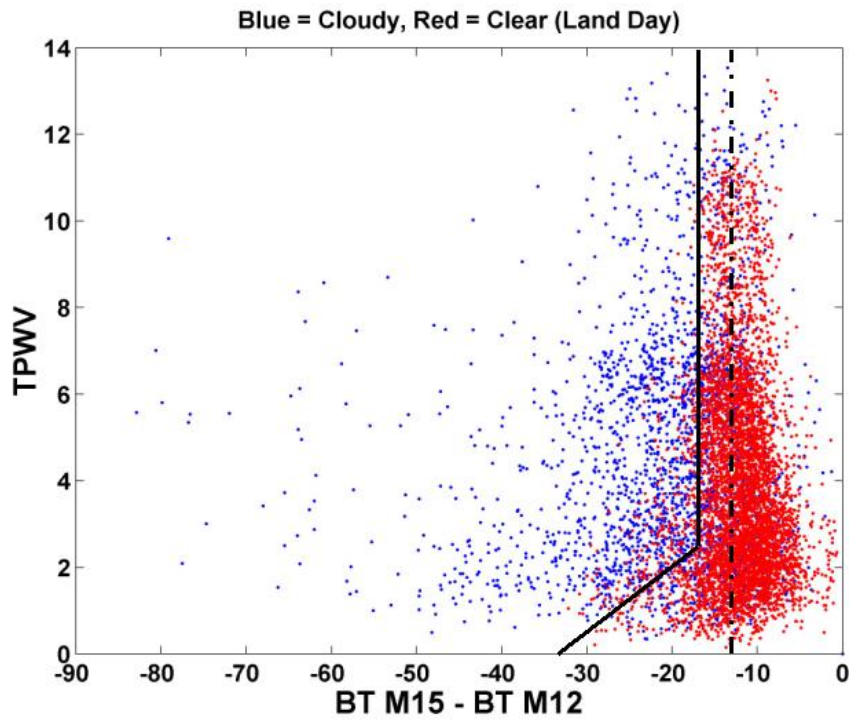
**Figure 4. MODIS granules used to assess performance of the VIIRS Daytime Cloud Mask Algorithm. (Note: some clouds may be indiscernible in the color composites.)**



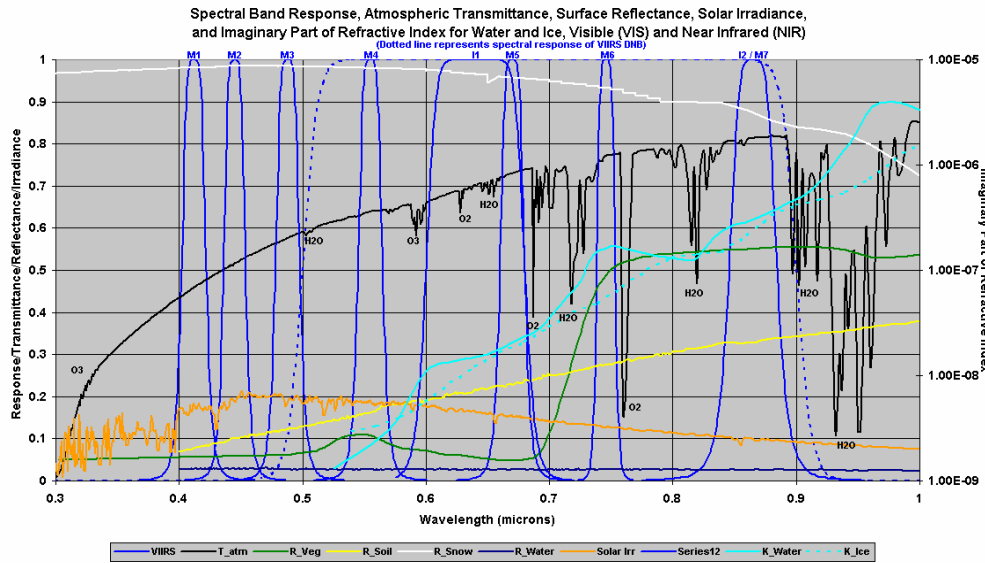
**Figure 5. Pre-Launch Implementation of VIIRS Spatial Tests for Cloud Detection over Ocean Surfaces in MODIS Data.**



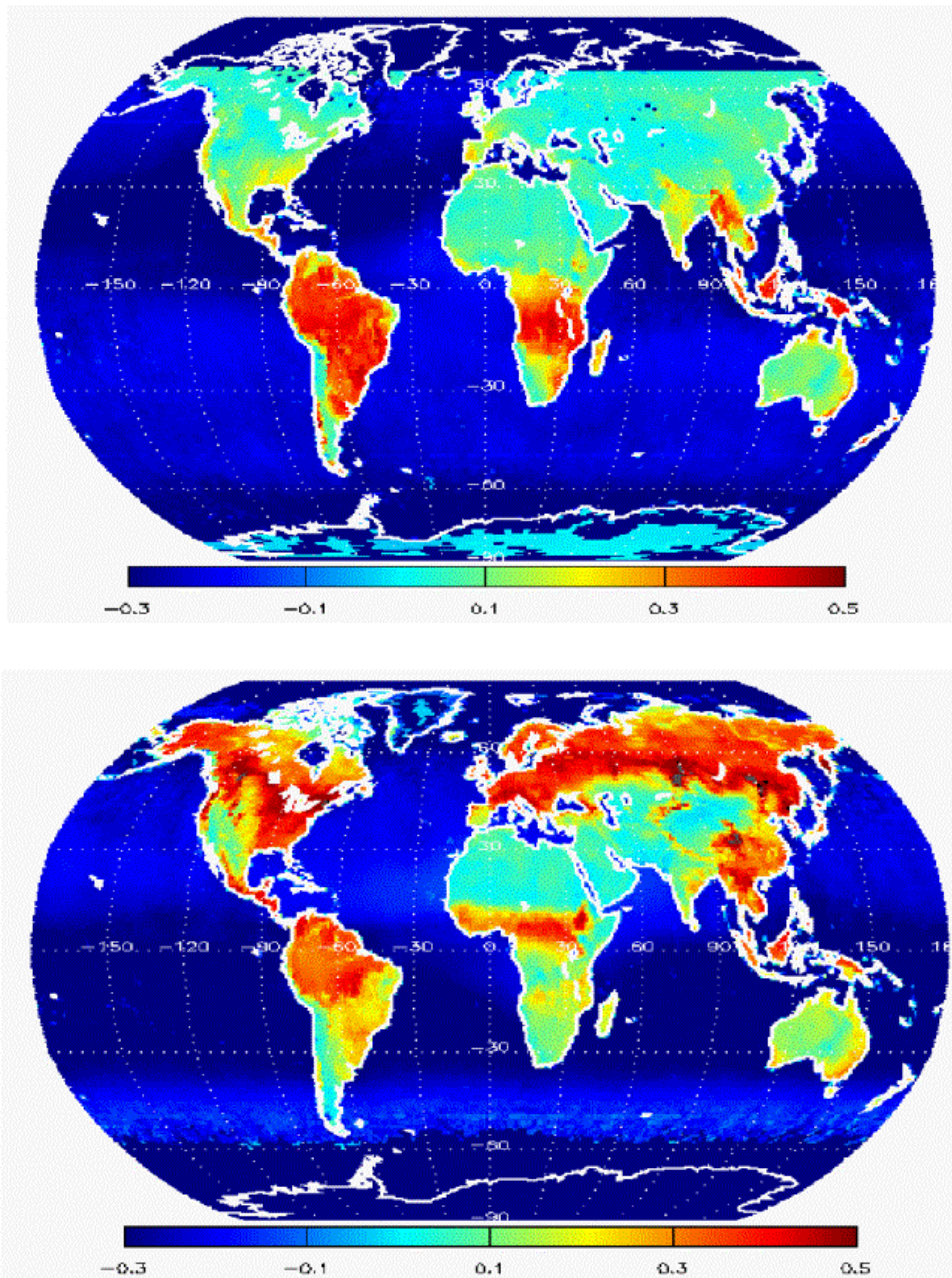
**Figure 6. Performance of the VIIRS Automated Cloud Analysis for the MODIS scene in shown Figure 4(e) using a spatial test based upon 0.865 $\mu$ m imagery channel. Manual analysis of clouds in MODIS scene in shown Figure 4(e) based upon human interpretation of imagery in Panel (a) with sun glint region shown in Panel (b). Automated cloud analysis in Panel © of MODIS scene in shown Figure 4(e) along with differences comparison with manual analysis from Panel (a) shown in Panel (d).**



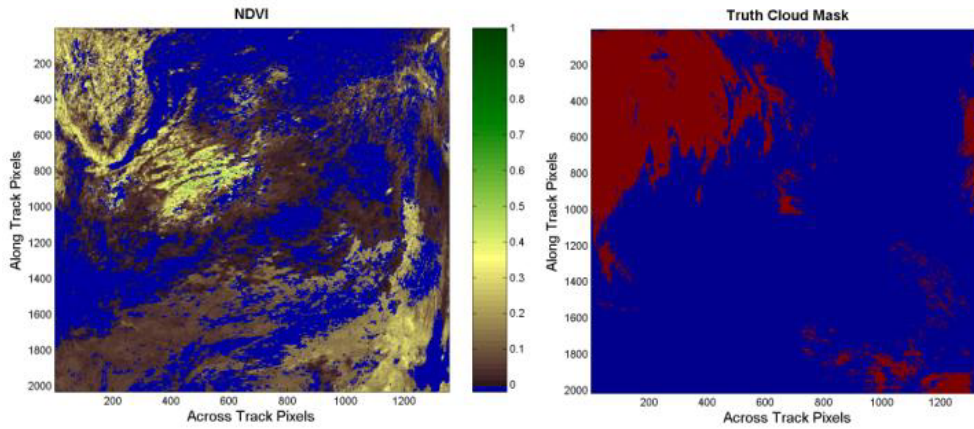
**Figure 7.** Observed B15-B12 BTD values found in the global synthetic data set for cloudy (red) and cloud-free (blue) pixels as a function of total precipitable water (TPW).



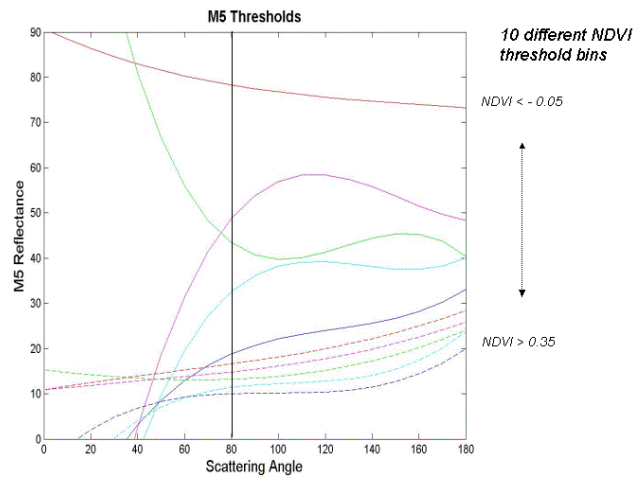
**Figure 8. Spectral signatures of cloud particles and surface backgrounds in 0.3 - 1.0 micron range. (Key: Reflectivities: vegetated land = green, ocean = dark blue, snow = white, bare soil or sand = yellow., solar illumination = gold and atmospheric transmission = black. VIIRS bands blue, solid turquoise = index of refraction for water droplets, and dashed turquoise = index of refraction for ice.)**



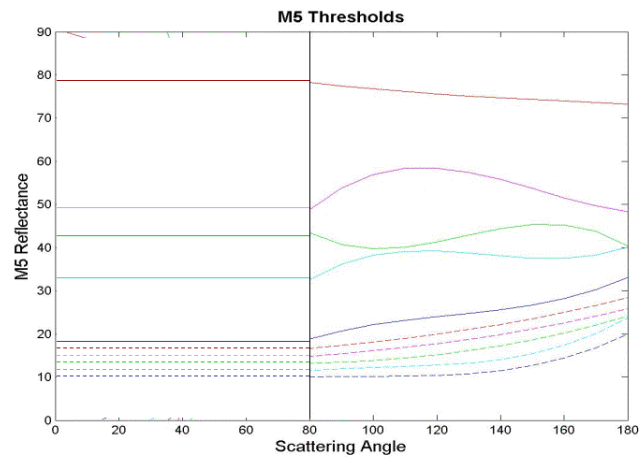
**Figure 9.** Typical changes in global NDVI fields during (a) January and (b) July due to variations in seasonal precipitation patterns (Heidinger, 2004).



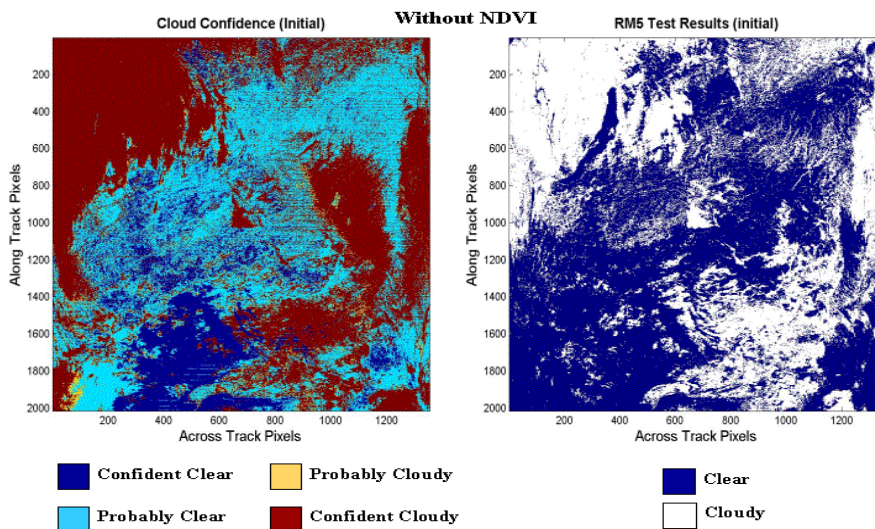
**Figure 10. NDVI field used in the of MODIS Scene A2002\_001\_0340 (left) along with manually generated cloud analyses used as truth in comparisons with VCM analyses (right).**



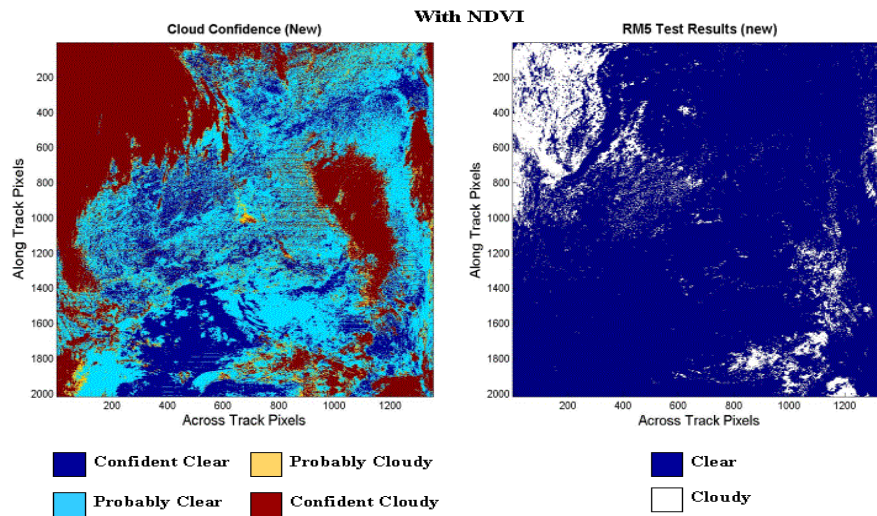
**Figure 11.** Logic for thresholds used with M5 Reflectance Test employs a 3-degree polynomial fit to curves shown for 10 NDVI bins that range from NDVI of  $-0.05$  through  $0.35$ , after CLAVR.



**Figure 12. Logic for thresholds used with M5 Reflectance Test within the Daytime VCM algorithm allows the test to be evaluated with data collected in the terminator orbit.**



**Figure 13. Cloud confidence (left) based upon the original VCM algorithm along with results of the M5 Reflectance Test (right). No NDVI data base was used in this analysis and the VCM used M5 Reflectance Test thresholds shown in Table 4.)**



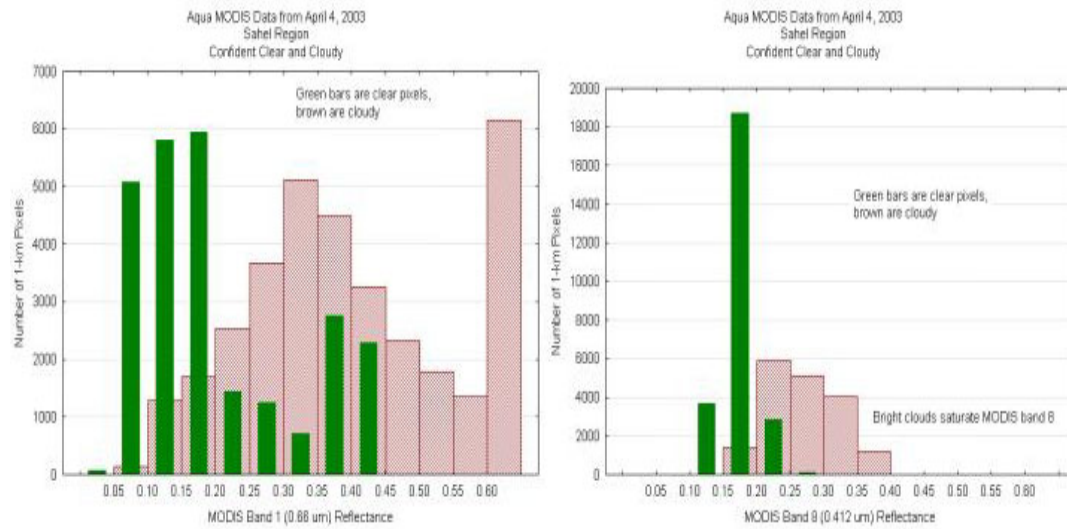


**Figure 15. Reflectance in the M5 band (left) and M1 band (right) for pixels classified as cloud-free (green) and cloudy (red) by the MODIS cloud mask algorithms.**